JOURNAL OF Materials CHEMISTRY

Crystal structures and magnetic properties of acid–base molecular complexes, (*p*-pyridyl nitronylnitroxide)$_2$X (X = hydroquinone, fumaric acid and squaric acid)

Takeo Otsuka,[a] Tsunehisa Okuno,[a] Kunio Awaga*[,a,c] and Tamotsu Inabe[b]

[a]*Department of Basic Science, Graduate School of Arts and Sciences, The University of Tokyo, Komaba, Meguro, Tokyo 153, Japan*

[b]*Division of Chemistry, Graduate School of Science, Hokkaido University, Sapporo 060, Japan*

[c]*Structure and Transformation, PRESTO, Japan Science and Technology Corporation (JST), Japan*

The reactions of 2-(4-pyridyl)-4,4,5,5-tetramethyl-4,5-dihydro-1*H*-imidazol-1-oxyl 3-*N*-oxide (or *p*-pyridyl nitronylnitroxide, abbreviated as *p*-PYNN) with the three dibasic organic acids, X [=fumaric acid (FA), squaric acid (SA) and hydroquinone (HQ)], result in the formation of hydrogen-bonding complexes of (*p*-PYNN)$_2$·X composition. In their crystals, the organic acids make selective hydrogen bonds to the two kinds of hydrogen-bond accepting sites in *p*-PYNN; (*a*) the oxygen atom in the NO group and (*b*) the nitrogen atom of the pyridyl ring. *p*-PYNN$_2$·HQ crystallizes in the monoclinic $P2_1/n$ space group. The HQ molecule bridges two *p*-PYNNs, and selects site (*a*) in *p*-PYNN as the hydrogen bond acceptor [*i.e.* (*p*-PYNN)NO···HO(HQ)OH···ON(*p*-PYNN)]. *p*-PYNN$_2$·FA crystallizes in the monoclinic $P2_1/n$ space group. The FA molecule connects two *p*-PYNN molecules with an intermolecular hydrogen bond to site (*b*) [(*p*-PYNN)N···HO(FA)OH···N(*p*-PYNN)]. The 2:1 compound of *p*-PYNN and SA crystallizes with the crystal solvent, 1,4-dioxane (abbreviated as diox), in the formula for *p*-PYNN$_2$·SA·diox. The crystal belongs to the triclinic $P\bar{1}$ space group. The SA molecule occupies the space between two *p*-PYNNs, making contact with site (*b*), as FA does in the *p*-PYNN$_2$·FA crystal. However the structure of SA indicates that it is a dianion in which the two protons are missing and, thus, the hydrogen bond is ionic [(*p*-PYNN)NH$^+$···O$^-$(SA)O$^-$···H$^+$N(*p*-PYNN)]. The selectivity and features of the hydrogen bonds can be qualitatively understood in terms of competition between the electrostatic and charge-transfer terms in the hydrogen-bonding energy, which is governed by the acidity of the organic acids and the proton accepting abilities of the two sites in *p*-PYNN. The three molecular compounds exhibited different antiferromagnetic properties, which depend on the mutual arrangement of *p*-PYNN in the crystals. The intermolecular interactions were interpreted based on the McConnell's spin polarization mechanism.

It is widely accepted that hydrogen bonding can influence intermolecular arrangements in the condensed state containing organic molecules and recently, this has been recognised as a key factor in supramolecular chemistry[1] for designing and synthesizing molecular aggregates with fundamental structural, symmetry, topology, and network properties, and for applications,[2] such as non-linear optics, ferromagnetism, ferroelectricity, liquid crystals, and electronics. Hydrogen bonding is not only the main factor in determining solid state structures but is also the microscopic origin of physical properties.[3] It is important to study the patterns, topology, selectivity, and the strength of hydrogen bonds, that are dependent on the hydrogen-bonding abilities of organic functional groups and on the steric (size and shape) effects of molecules. While most research has been based on the measurement of solution association constants under equilibrium conditions,[4] extraction of the hydrogen-bonding patterns from a wide variety of crystallographic data was performed by Etter *et al.*[5] Crystallographic studies are advantageous in the analysis of hydrogen-bond selectivity in complex systems such as the 2-aminopyrimidine-carboxylic acid compounds, which involve multiple hydrogen bonds.[5]

In the field of molecular magnetic materials, the idea of making use of intermolecular hydrogen bonds to get ferromagnetic intermolecular interactions, has been tested by Veciana[6] and Sugawara[7] *et al.* In addition, we have observed the coexistence of organic radicals and naked protons in the solid state: the reaction of 2-(3-pyridyl)- or 2-(4-pyridyl)-4,4,5,5-tetramethyl-4,5-dihydro-1*H*-imidazol-1-oxyl 3-*N*-oxide (abbreviated as *m*- or *p*-PYNN, respectively) and HBr gas leads to the 2:1 complex, (*m*-PYNN)$_2$·HBr or (*p*-PYNN)$_2$·HBr.[8] Although single crystals were not obtained, IR spectra strongly indicated proton sharing between the two pyridyl rings, *i.e.* an intermolecular [NHN]$^+$ hydrogen bond. This type of situation may lead to cooperative phenomena between magnetism and proton dynamics in the future.

In this paper, we describe the crystal structures and the magnetic properties of three acid–base molecular compounds: *p*-PYNN$_2$·HQ, *p*-PYNN$_2$·FA and *p*-PYNN$_2$·SA·diox. We analyzed their crystal structures, focusing on selectivity and the features of the hydrogen bonds. The observed selectivity in the hydrogen bonds was interpreted in terms of competition between the electrostatic and the charge-transfer terms in the hydrogen bonding energy. In addition, the likelihood of molecular recognition in the hydrogen-bonding formation was analyzed.

Experimental

p-PYNN was prepared according to the procedure previously described.[9] HQ, FA and SA were of reagent grade and were used as commercially obtained. The molecular compounds, *p*-PYNN$_2$·HQ and *p*-PYNN$_2$·FA were prepared as follows: *p*-PYNN and HQ (or FA) in 2:1 proportion were dissolved in acetone at 40 °C, and their crystals were grown with slow evaporation of the solvent at 0 °C. The molecular compound of *p*-PYNN and SA was obtained following the same procedure using water–dioxane (2:1) instead of acetone. Crystallization took place with dioxane to give *p*-PYNN$_2$·SA·diox. Selected IR data $\bar{\nu}$/cm^{-1} (KBr): 3232 (m, br; OH st.), 1596 (m; pyridyl

ring st.) for $PYNN_2 \cdot HQ$; 2440 and 1933 (m, br; OH st.), 1603 (m; pyridyl ring st.) for *p*-$PYNN_2 \cdot FA$; 2574 (m, br; NH st.), 1630 (m; pyridyl ring st.) for *p*-$PYNN_2 \cdot SA \cdot diox$.

X-Ray diffraction data were collected on a Rigaku AFC-5S (*p*-$PYNN_2 \cdot HQ$ and *p*-$PYNN_2 \cdot SA \cdot diox$) or a Mac Science MXC18 (*p*-$PYNN_2 \cdot FA$) automatic four-circle diffractometer with graphite-monochromatized Mo-Kα radiation ($\lambda =$ 0.71073 Å). Unit cell dimensions were obtained by a least-squares refinement, using 25 reflections with $20^\circ < 2\theta < 25^\circ$ for *p*-$PYNN_2 \cdot HQ$ and *p*-$PYNN_2 \cdot SA \cdot diox$, or using 26 reflections with $30^\circ < 2\theta < 35^\circ$ for *p*-$PYNN_2 \cdot FA$. During data collection, the intensities of three representative reflections were measured as a check on crystal stability, and no loss was observed. No absorption correction was performed, because the influence of the absorption was negligible. The crystal structures were solved by direct methods (SHELXS-86[10] and DIRDIF[11]). Block-matrix-diagonalization least-squares refinement (UNICS-III[12]) with anisotropic thermal parameters for all non-hydrogen atoms was employed for *p*-$PYNN_2 \cdot SA \cdot diox$ and *p*-$PYNN_2 \cdot HQ$. The positions of the hydrogen atoms were found by differential Fourier methods and they were refined isotropically with a fixed thermal parameter in order to avoid an excessive number of parameters. A refinement for the non-hydrogen atoms in *p*-$PYNN_2 \cdot FA$ was performed by using the full-matrix least-squares method with anisotropic thermal parameters. The positions of the hydrogen atoms were calculated, and were refined with isotropic thermal parameters at a geometrically restrained position. Details in regards to the crystallographic parameters are given in Table 1. Full crystallographic details excluding structure factors have been deposited at the Cambridge Crystallographic Data Centre (CCDC). See Information for Authors, *J. Mater. Chem.*, 1998, Issue 1. Any request to the CCDC for this material should quote the full literature citation and the reference number 1145/85.

Static magnetic susceptibilities and magnetization were measured in a 1 T field on a Faraday balance, which has been previously described.[13] The temperature dependence of the magnetic susceptibility was examined at 3–280 K.

Molecular orbital calculations were performed with the MOPAC package,[14] in order to estimate the atomic charges and the spin densities on *p*-PYNN.

Crystal structures

p-$PYNN_2 \cdot HQ$

The 2:1 complex of *p*-PYNN and HQ crystallizes in the monoclinic $P2_1/n$ space group. The structure of the *p*-$PYNN_2 \cdot HQ$ unit is shown in Fig. 1, in which half of the unit is crystallographically independent. The selected bond distances and angles are listed in Table 2. The HQ molecule bridged the NO groups of separate *p*-PYNNs with a hydrogen bond. The intermolecular distance between O(1)···O(18) is 2.728(5) Å. This type of hydrogen bond has been observed in the complex of phenylboronic acid and phenyl nitronylnitroxide: *viz*. the acid bridge in the NO groups of the nitronylnitroxide in the solid state.[15]

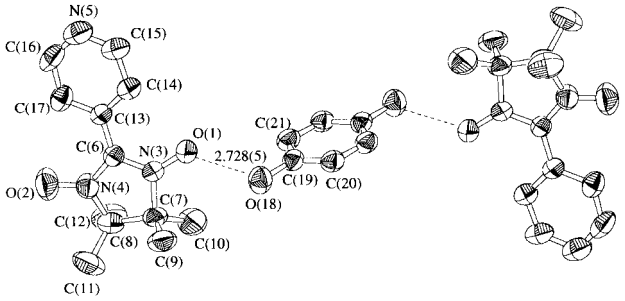

Fig. 1 Molecular structures in the *p*-$PYNN_2 \cdot HQ$ unit

Table 3 shows the atomic charges on the skeleton of *p*-PYNN calculated using the geometry in the bulk crystal.[16] Table 3 also shows the calculated spin densities. As a common characteristic of the nitronylnitroxide radical family, the positive spin densities are concentrated on the NO groups since the oxygen atom in the NO group has the largest negative charge. The spin polarization slightly penetrates the aromatic substituent at the α carbon (the pyridyl ring) and alternation of the positive and negative spin densities is observed on the skeleton.

Fig. 2(*a*) and (*b*) show projections of the crystal structure of *p*-$PYNN_2 \cdot HQ$ parallel and perpendicular to the *b* axis, respectively. In Fig. 2(*b*) the HQ molecules are omitted for the sake of clarity. There is a one-dimensional stacking column of *p*-PYNN along the *b* axis, in which the molecules are arranged head-to-tail. In the intermolecular arrangement, the short intermolecular distances are 3.370(7) for O(1)···C(16)^{i} and 3.347(6) Å for N(5)···C(6)^{i} [symmetry operation; (i) $0.5-x$, $y+0.5$, $0.5-z$]. The former indicates a spatial overlap between the positive spin densities on the neighboring molecules and the latter between the negative spin densities. According to McConnell's spin polarization mechanism,[17] these kinds of overlaps between polarized spin densities of the same sign are expected to result in an antiferromagentic coupling. Since the stacking columns are separated from each other by the HQ

Table 1 Crystal data and experimental conditions for *p*-$PYNN_2 \cdot HQ$, *p*-$PYNN_2 \cdot FA$ and *p*-$PYNN_2 \cdot SA \cdot diox$

compound	$PYNN_2 \cdot HQ$	$PYNN_2 \cdot FA$	$PYNN_2 \cdot SA \cdot diox$
formula	$C_{30}H_{36}O_6N_6$	$C_{28}H_{36}O_8N_6$	$C_{32}H_{42}O_{10}N_6$
formula weight	578.67	584.63	670.72
crystal system	*monoclinic*	*monoclinic*	*triclinic*
space group	$P2_1/n$	$P2_1/n$	$P\bar{1}$
a/Å	26.24(1)	14.970(5)	8.988(2)
b/Å	6.806(2)	7.552(2)	13.011(4)
c/Å	8.330(3)	13.090(5)	7.894(3)
α(°)			93.69(3)
β(°)	94.61(3)	92.58(3)	102.58(3)
γ(°)			109.82(2)
V/Å^3	1480.0(9)	1478.5(8)	837.9(5)
Z	2	2	1
D_c/g cm^{-3}	1.299	1.310	1.329
radiation	Mo-Kα ($\lambda = 0.71073$ Å, graphite monochromator)		
2θ range (°)	55	60	55
measured	3658	4809	4176
observed	1542	2250	3555
R	0.0677	0.0691	0.0531
R_w	0.0602	0.0823	0.0541

Table 2 Selected bond lengths (Å) and angles (°) for *p*-$PYNN_2 \cdot HQ$

	bond length/Å				
O(1)—N(3)	1.277(6)	O(2)—N(4)	1.284(5)	N(3)—C(6)	1.350(6)
N(4)—C(6)	1.343(5)	C(6)—C(13)	1.456(6)	C(13)—C(14)	1.392(6)
C(14)—C(15)	1.390(7)	C(15)—N(5)	1.327(7)	N(5)—C(16)	1.321(6)
C(16)—C(17)	1.385(7)	C(13)—C(17)	1.401(6)	O(18)—C(19)	1.383(5)
C(19)—C(20)	1.385(6)	C(19)—C(21)	1.377(6)		

	bond angle (°)		
O(1)—N(3)—C(6)	126.4(4)	O(2)—N(4)—C(6)	125.5(4)
N(3)—C(6)—N(4)	107.8(4)	C(14)—C(13)—C(17)	117.2(4)
C(13)—C(14)—C(15)	118.0(4)	N(5)—C(15)—C(14)	125.5(5)
C(15)—N(5)—C(16)	115.7(4)	N(5)—C(16)—C(17)	124.8(4)
C(16)—C(17)—C(13)	118.8(4)	O(18)—C(19)—C(20)	116.9(4)
O(18)—C(19)—C(21)	123.4(4)	C(20)—C(19)—C(21)	119.7(4)
C(19)—C(20)—C(21)^{i}	119.2(4)	C(19)—C(21)—C(20)^{i}	121.0(4)

(*i*) Symmetry operation; $\bar{x}-1$, $\bar{y}$, $\bar{z}-1$.

Table 3 Atomic charge and spin density distribution on *p*-PYNN as obtained by the PM3-UHF method

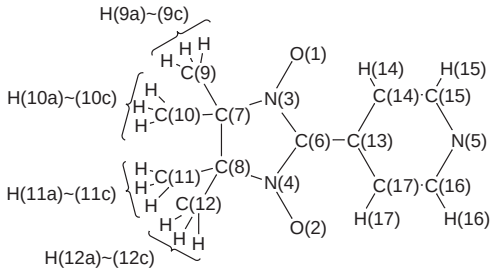

atom(s)	atomic charges	spin densities
O(1), O(2)	−0.53200	0.33102
N(3), N(4)	0.68960	0.43052
N(5)	−0.04680	−0.18245
C(6)	−0.43240	−0.50487
C(7), C(8)	−0.14115	0.02126
C(9), C(11)	−0.06480	0.00950
C(10), C(12)	−0.08155	0.01297
C(13)	0.03010	0.26929
C(14), C(17)	−0.10165	−0.25617
C(15), C(16)	−0.06480	0.20464
H(9a)~(9c), H(11a)~(11c)	0.04785	−0.00069
H(10a)~(10c), H(12a)~(12c)	0.05150	−0.00079
H(14), H(17)	0.12180	0.01451
H(15), H(16)	0.10065	−0.01229

molecules, the magnetic interaction between the columns would be very weak.

p-$PYNN_2 \cdot FA$

The structure of *p*-$PYNN_2 \cdot FA$ belongs to the monoclinic $P2_1/n$ space group. The geometry of *p*-$PYNN_2 \cdot FA$ is shown in Fig. 3. Selected bond distances and angles are listed in Table 4. The organic acid FA occupies the space between the pyridyl rings of *p*-PYNNs. There is an intermolecular hydrogen bond between the OH group of FA and the nitrogen atom [*i.e.* N(5)] on the pyridyl ring of *p*-PYNN, although N(5) is less electronegative than O(1) and O(2) in the NO groups (see Table 3). The charge-transfer term would contribute to the hydrogen bond contact here, as will be discussed later. The intermolecular, interatomic distance between N(5)···O(18) is 2.634(2) Å, indicating the presence of a strong hydrogen bond. The asymmetric bond distances in the CO_2 moiety of FA [1.317(4) Å for C(21)–O(18) and 1.208(4) Å for C(21)–O(19)] indicate that the hydrogen on the intermolecular N···O distance remains on the side of FA (*i.e.* O—H···N). This is further supported by the fact that the IR spectrum shows two broad ν(OH) stretching bands at 2440 and 1933 cm^{-1}. Usually,

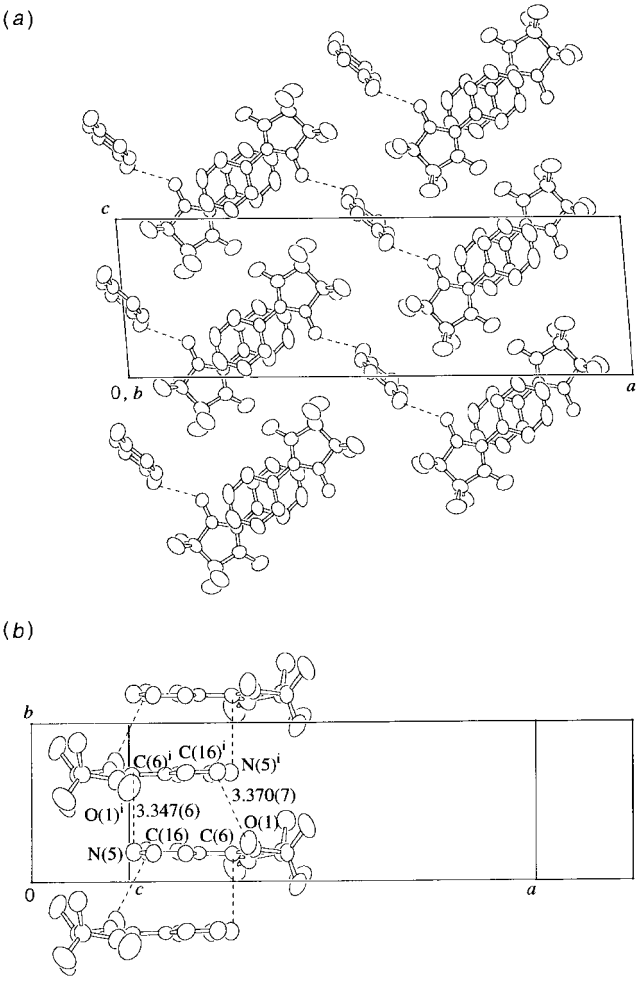

Fig. 2 Projection of the crystal structure of *p*-$PYNN_2 \cdot HQ$ (*a*) parallel to the *b* axis and (*b*) perpendicular to the *b* axis [symmetry operation: (i) $0.5-x$, $y+0.5$, $0.5-z$]

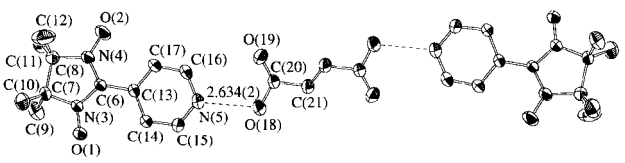

Fig. 3 Molecular structures in the *p*-$PYNN_2 \cdot FA$ unit

Table 4 Selected bond lengths (Å) and angles (°) for *p*-$PYNN_2 \cdot FA$

	bond length/Å				
O(1)—N(3)	1.279(4)	O(2)—N(4)	1.274(4)	N(3)—C(6)	1.351(3)
N(4)—C(6)	1.353(3)	C(6)—C(13)	1.465(3)	C(13)—C(14)	1.397(3)
C(14)—C(15)	1.388(4)	C(15)—N(5)	1.334(4)	N(5)—C(16)	1.334(4)
C(16)—C(17)	1.386(4)	C(13)—C(17)	1.398(3)	O(18)—C(20)	1.317(4)
O(19)—C(20)	1.208(4)	C(20)—C(21)	1.491(4)	C(21)—$C(21)^{i}$	1.307(4)

	bond angle (°)		
O(1)—N(3)—C(6)	126.2(2)	O(2)—N(4)—C(6)	126.1(3)
N(3)—C(6)—N(4)	108.3(2)	C(14)—C(13)—C(17)	118.2(2)
C(13)—C(14)—C(15)	118.3(3)	N(5)—C(15)—C(14)	123.8(3)
C(15)—N(5)—C(16)	117.5(3)	N(5)—C(16)—C(17)	123.5(3)
C(16)—C(17)—C(13)	118.6(3)	O(18)—C(20)—O(19)	124.2(3)
O(18)—C(20)—C(21)	112.6(2)	O(19)—C(20)—C(21)	123.2(3)
C(20)—C(21)—$C(21)^{i}$	122.3(3)		

(*i*) Symmetry operation; $1-x$, $1-y$, $1-z$.

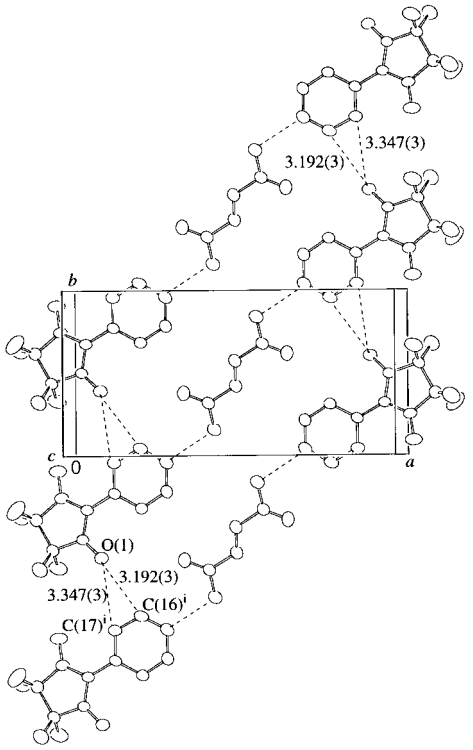

Fig. 4 Projection of the crystal structure of *p*-$PYNN_2 \cdot FA$ onto the *ab* plane [symmetry operation: (i) x, $y-1$, z]

these bands are observed in a strongly asymmetric, double-minimum hydrogen bond in complexes of carboxylic acids and pyridines.[18]

Fig. 4 shows a projection of the crystal structure on to the *ab* plane. The *p*-PYNN molecules show side-by-side and head-to-head stacking along the *b* axis. The short distances in the stacking are 3.192(3) Å for O(1)···$C(16)^{i}$ and 3.347(3) Å for O(1)···$C(17)^{i}$ [symmetry operation; (i) x, $y-1$, z]. There are hydrogen bonds between O(1) in the NO group and the hydrogen atoms, $H(16)^{i}$ and $H(17)^{i}$, on the pyridyl ring. The contact O(1)···$H(16)^{i}$ is an overlap between the positive and negative spin densities, while the contact O(1)···$H(17)^{i}$ is one between the positive spin densities. The magnetic interactions appear to be competing in this arrangement. The two-dimensional sheet shown in Fig. 4 is stacked along the *c* axis with a screw relationship. There was no significant contact in the intersheet arrangement.

p-$PYNN_2 \cdot SA \cdot diox$

The adduct crystallizes in the triclinic $P\bar{1}$ space group. Fig. 5 shows the structure of the *p*-$PYNN_2 \cdot SA \cdot diox$ unit. Selected

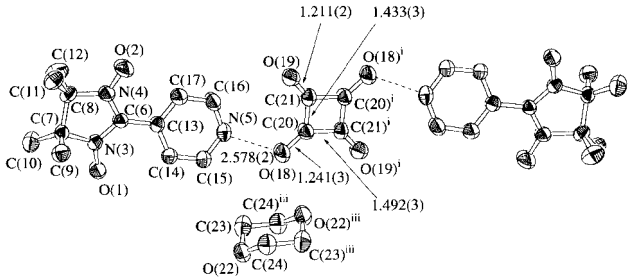

Fig. 5 Molecular structures in the *p*-$PYNN_2 \cdot SA \cdot diox$ unit [symmetry operation: (i) $\bar{x}$, $1-y$, $1-z$]

bond distances and angles are listed in Table 5. The SA molecule bridges the gap between the pyridyl rings of the *p*-PYNNs, as well as FA in *p*-$PYNN_2 \cdot FA$. The intermolecular, interatomic distance N(5)···O(18) is 2.578(2) Å, which is shorter than that in *p*-$PYNN_2 \cdot FA$. It is significant that the two oxygen atoms of the SA molecule which are attached to two separate *p*-PYNN molecules are diagonal to each other, and not adjacent to each other. In addition, the SA molecule is on a crystallographic inversion symmetry centre and has little bond alternation: the bond distances C(20)—O(18) and C(21)—O(19) are 1.241(3) and 1.211(2) Å, respectively, and C(20)—C(21) and C(20)—$C(21)^{i}$ are 1.433(3) and 1.492(3) Å, respectively [symmetry operation; (i) $\bar{x}$, $1-y$, $1-z$]. The structure and coordination of SA indicate that the molecule is a squarate dianion in which the two protons are missing and the proton in the N···O intermolecular contact is attached to *p*-PYNN (*i.e.* $O^{-} \cdots H^{+}\text{-}N^{-}$).

Fig. 6 shows the structure of *p*-$PYNN_2 \cdot SA \cdot diox$. In the crystal, *p*-PYNN acts as a dimer with a short distance between the NO groups: the distances O(1)···$O(1)^{ii}$ and O(1)···$N(3)^{ii}$ are 3.667(2) and 3.658(2) Å, respectively [symmetry operation; (ii) $\bar{x}-1$, $\bar{y}$, $z-1$]. Since the positive spin densities are concentrated on the NO groups, there would be a large overlap between them, thereby resulting in antiferromagnetic coupling in the dimer. The arrangement resembles that of *p*-*N*-methylpyridinium nitronylnitroxide (abbreviated as *p*-MPYNN) in its iodide salt.[19] *p*-MPYNN has a substituent (methyl group) at the pyridyl nitrogen atom and a positive charge on the pyridinium ring, as well as the *N*-protonated *p*-PYNN in *p*-$PYNN_2 \cdot SA \cdot diox$. The arrangement of *p*-MPYNN in *p*-MPYNN·I resulted in a strong antiferromagnetic coupling.[19]

Selectivity in hydrogen bonds of *p*-PYNN

The crystal structures of the 2:1 molecular complexes of *p*-PYNN and three organic acids with different acidity have been examined. The three acids formed different hydrogen bonds with *p*-PYNN, which involved two hydrogen-bond accepting sites: (*a*) the oxygen in the NO group and (*b*) the nitrogen on

Table 5 Selected bond lengths (Å) and angles (°) for *p*-$PYNN_2$·SA·diox[a]

	bond length/Å				
O(1)—N(3)	1.274(2)	O(2)—N(4)	1.275(3)	N(3)—C(6)	1.353(2)
N(4)—C(6)	1.354(3)	C(6)—C(13)	1.459(3)	C(13)—C(14)	1.385(3)
C(14)—C(15)	1.371(3)	C(15)—N(5)	1.333(3)	N(5)—C(16)	1.335(3)
C(16)—C(17)	1.370(3)	C(13)—C(17)	1.400(3)	O(18)—C(20)	1.241(3)
O(19)—C(21)	1.211(2)	C(20)—C(21)	1.433(3)	C(20)—C(21)^{i}	1.492(3)
O(22)—C(23)	1.426(3)	O(22)—C(24)	1.417(3)	C(23)—C(24)^{iii}	1.503(3)

	bond angle (°)		
O(1)—N(3)—C(6)	127.1(2)	O(2)—N(4)—C(6)	126.2(2)
N(3)—C(6)—N(4)	108.4(2)	C(14)—C(13)—C(17)	118.1(2)
C(13)—C(14)—C(15)	119.5(2)	N(5)—C(15)—C(14)	121.3(2)
C(15)—N(5)—C(16)	120.7(2)	N(5)—C(16)—C(17)	120.9(2)
C(16)—C(17)—C(13)	119.5(2)	O(18)—C(20)—C(21)	134.1(2)
O(18)—C(20)—(21)^{i}	134.5(2)	C(21)—C(20)—C(21)^{i}	91.4(2)
O(19)—C(21)—C(20)	135.3(2)	O(19)—C(21)—C(20)^{i}	136.1(2)
C(20)—C(21)—C(20)^{i}	135.3(2)	C(23)—O(22)—C(24)	109.6(2)
O(22)—C(23)—C(24)^{iii}	110.4(2)	O(22)—C(24)—C(23)^{iii}	111.0(2)

[a](i) Symmetry operation; $\bar{x}-1, 1-y, 1-z$: (iii) Symmetry operation; $1-x, 1-y, z$.

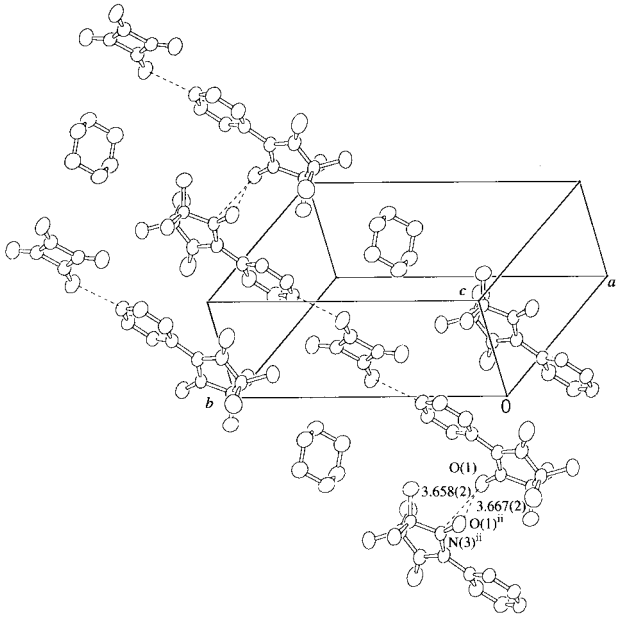

Fig. 6 View of the crystal structure of *p*-$PYNN_2$·SA·diox [symmetry operation: (ii) $\bar{x}-1, \bar{y}, \bar{z}-1$]

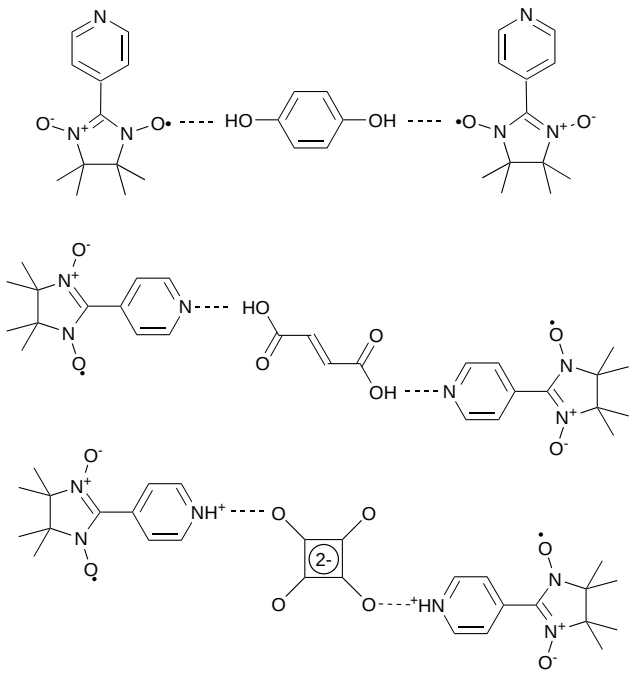

Scheme 1

the pyridyl ring. The features of the hydrogen bonds in the three are shown in Scheme 1.

The acidic hydrogen of HQ attached to site (*a*) (O—H···O), while FA and SA selected site (*b*). In addition, the hydrogen bond in *p*-$PYNN_2$·FA is neutral (O—H···N), while that in *p*-$PYNN_2$·SA·diox is ionic ($O^-\cdots H^+$—N). The distance between the two atoms connected by the hydrogen bond becomes longer in the order *p*-$PYNN_2$·HQ, *p*-$PYNN_2$·FA, *p*-$PYNN_2$·SA·diox.

The nature of the hydrogen bond [A—H···B] can be expressed on the whole by the following five configurations:[20]

1 A—H···B
2 A^-—H^+···B
3 A^+—H^-···B
4 $A^-\cdots H^+$—B
5 A···H^-—B^+

Structures **1**, **2** and **3** produce the electrostatic stabilization energy E_{EL} of the hydrogen bond, while structures **4** and **5** cause the charge transfer stabilization E_{CT}. Since HQ is a very weak acid, electrostatic stabilization terms **1**, **2** and **3** play a dominant role in the hydrogen bonds of HQ, and the contributions of **4** and **5** which are given by the dissociation of the A—H bond must be small. Therefore, the more electronegative oxygen in the NO group of *p*-PYNN would be chosen as the hydrogen-bond acceptor in the crystal of *p*-$PYNN_2$HQ. On the other hand, FA and SA are much stronger acids than HQ, and the E_{CT} in their hydrogen bonds which is produced by configurations **4** and **5** must be larger than that in the hydrogen bond of HQ. Here, the binding energies of the H—B bonds in the CT states govern the hydrogen bonds. With regard to the two hydrogen-bond acceptors in *p*-PYNN, the binding energy of the H^+—N bond at site (*b*) would be larger than that of the H—ON bond at (*a*). Therefore strong acids are considered to prefer site (*b*) to (*a*) as a hydrogen bond acceptor. This is why site (*b*) was chosen in the crystals of *p*-$PYNN_2$·FA and *p*-$PYNN_2$·SA·diox. The hydrogen bond in *p*-$PYNN_2$·FA is neutral and the acidic hydrogen remains in FA. This indicates that E_{EL} is still effective in *p*-$PYNN_2$·FA, in addition to E_{CT}. The hydrogen bond in *p*-$PYNN_2$·SA·diox is ionic, indicating the superiority of E_{CT} over E_{EL}. The pK_a difference between the pyridinium ions and the carboxylic acids in aqueous solution, which is denoted as ΔpK_a, was used to analyze the hydrogen bonds in various pyridine–carboxylic acid complexes in solution or even in the solid state.[18] The hydrogen bond would be ionic when $\Delta pK_a > 3.75$, and would be neutral when it is less than that value. The selectivity and features of the hydrogen bonds in the three molecular compounds of *p*-PYNN

can be qualitatively explained in terms of the competition between E_{EL} and E_{CT} in the hydrogen bonds, which depends on the acidity of the organic acids and on the binding energy of hydrogen to the two hydrogen bond accepting sites in *p*-PYNN.

Magnetic properties

The temperature dependences of the magnetic susceptibilities of the three compounds were examined in the temperature range 3–280 K. The correction for the diamagnetic contribution was performed by using the diamagnetic susceptibilities that were evaluated assuming that the paramagnetic component follows the Curie law at high temperatures. The paramagnetic susceptibilities, χ_p, obtained are shown in Fig. 7, where the molar unit is defined as half of the *p*-$PYNN_2 \cdot X$ unit and a logarithmic scale was used in order to clarify the low-temperature behavior.

The open circles in Fig. 7 show the temperature dependence of χ_p for *p*-$PYNN_2 \cdot HQ$. The value of χ_p increases with a decrease in temperature to 5 K and, after reaching a maximum, it decreases with a further decrease in temperature. Below 5 K, χ_p approaches a non-zero value at absolute zero. The behavior can be interpreted in terms of an antiferromagnetic one-dimensional chain,[21] using eqn. (1);

$$\chi = \frac{4C}{T}\frac{a_0 + a_1 x + a_2 x^2}{1 + a_3 x + a_4 x^2 + a_5 x^3} \quad (1)$$

$$\text{with } x = |J|/2k_B T,$$

constants a_0–a_5 have been defined elsewhere,[22] $|J|$ is the magnitude of intrachain magnetic coupling, C the Curie constant and k_B the Boltzmann constant. The solid curve in Fig. 7 which goes through the plots for *p*-$PYNN_2 \cdot HQ$ is the best theoretical fit for eqn. (1) with parameters $|J|/k_B = 4.7$ K and $C = 0.376$ emu mol^{-1} (fixed). As described in the previous section, the *p*-PYNN radicals form a one-dimensional stacking column along the *b* axis in *p*-$PYNN_2 \cdot HQ$ (see Fig. 2). The stack should be assigned to the antiferromagnetic chain.

The squares in Fig. 7 show the results of *p*-$PYNN_2 \cdot FA$. The value of χ_p gradually increases with a decrease in temperature in the temperature range studied. This behavior can be interpreted in terms of the Curie–Weiss law. The solid curve which was fitted to the plots for *p*-$PYNN_2 \cdot FA$ is the best theoretical fit of the Curie–Weiss law with a Curie constant of $C = 0.376$ emu (fixed) and a Weiss constant of $\theta = -0.68$ K. The weak magnetic interaction would be caused by the cancellation between the ferromagnetic and antiferromagentic contributions in the arrangement shown in Fig. 4.

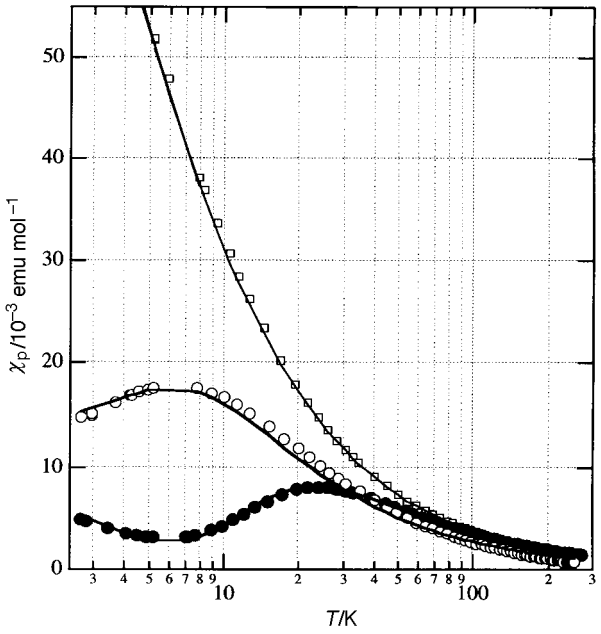

Fig. 7 Temperature dependences of the paramagnetic susceptibilities χ_p in a log scale for (○) *p*-$PYNN_2 \cdot HQ$, (□) *p*-$PYNN_2 \cdot FA$ and (●) *p*-$PYNN_2 \cdot SA \cdot diox$. The solid curves are theoretical ones (see the text).

The closed circles in Fig. 7 show χ_p for *p*-$PYNN_2 \cdot SA \cdot diox$. The value of χ_p increases with a decrease in temperature from 280 to 22 K; below that it shows a decrease. The increase of χ_p below 4 K would be caused by Curie spins on the lattice defects. Since *p*-PYNN exists as a dimer in the crystal of *p*-$PYNN_2 \cdot SA \cdot diox$, the temperature dependence of χ_p can be interpreted, as follows, based on the singlet–triplet model, eqn. (2);

$$\chi = \frac{4C}{T}\frac{\exp(2J/k_B T)}{1 + 3\exp(2J/k_B T)} + \frac{C_{def}}{T} \quad (2)$$

where J is the intradimer antiferromagnetic coupling constant and C_{def} is the Curie constant for the lattice defect. The solid curve that was fitted to the plots for *p*-$PYNN_2 \cdot SA \cdot diox$ in Fig. 7 is the best theoretical fit of eqn. (2) whose parameters are $J/k_B = -18.5$ K, $C = 0.376$ emu K mol^{-1} (fixed) and $C_{def} = 0.015$ emu K mol^{-1}. The theoretical curve can explain the observed behavior.

The three molecular compounds exhibited different magnetic properties. This reflects the difference in the molecular arrangements of *p*-PYNN in these compounds. Their intermolecular magnetic interactions can be understood in terms of the McConnell's spin polarization mechanism. Other researchers found that phenylboronic acid acts as a ferromagnetic spin-coupler in the molecular compound of (phenylboronic acid)(phenyl nitronylnitroxide) through an NO···HO—B—OH···ON pathway.[15] However, there is no suggestion of a magnetic interaction through the hydrogen bonds in the three compounds, even though HQ bridges the NO groups in *p*-$PYNN_2 \cdots HQ$. This could be responsible for the fact that the distances between the acidic hydrogen atoms are much longer in the three acids than in the boronic acid. As mentioned previously, the intermolecular arrangement between the protonated *p*-PYNNs in *p*-$PYNN_2 \cdot SA \cdot diox$ is similar to that of *p*-MPYNN in *p*-MPYNN·I. The *meta* derivative (*m*-MPYNN) exhibits a strong ferromagnetic intermolecular interaction on an unusual lattice named *Kagome*.[23] Research on protonated *m*-PYNN is now in progress.

Conclusion

We analyzed the crystal structures and the magnetic properties of the three acid–base molecular complexes, *p*-$PYNN_2 \cdot HQ$, *p*-$PYNN_2 \cdot FA$ and *p*-$PYNN_2 \cdot SA \cdot diox$. The organic acids formed selective hydrogen bonds to the two kinds of hydrogen-bond accepting sites in *p*-PYNN. The acidic hydrogen of HQ attached to the oxygen (O—H···O), while FA and SA selected the nitrogen on the pyridyl ring of *p*-PYNN. The hydrogen bond in *p*-$PYNN_2 \cdot FA$ was neutral (O—H···N), while that in *p*-$PYNN_2 \cdot SA \cdot diox$ was ionic ($O^- \cdots H^+ —N$). The hydrogen bonding patterns that we observed in the three crystals were qualitatively interpreted, in terms of the competition between the electrostatic stabilization and the charge-transfer stabilization in the hydrogen bond. This depends on the acidity of the organic acids and on the proton accepting abilities of the two sites in *p*-PYNN. The possibility of selective, controllable hydrogen-bond production is suggested. The three molecular compounds exhibit different antiferromagnetic properties, which are dependent on the intermolecular arrangement of *p*-PYNN in the crystals. Their magnetic couplings are explained, based on the McConnell's spin polarization mechanism.

This work was supported by a Grant-in-aid for Scientific

Research from the Ministry of Education, Science, and Culture, of the Japanese government.

References

1 *Comprehensive supramolecular chemistry*, ed. J. E. Davies, D. D. MacNicol and F. Vögtle, Pergamon, New York, 1996.
2 V. A. Russell, M. C. Etter and M. D. Ward, *Chem. Mater*., 1994, **6**, 1206.
3 Y. Moritomo, Y. Tokura, N. Nagaosa, T. Suzuki and K. Kumagai, *Phys. Rev. Lett*., 1993, **25**, 2833.
4 R. Langner and G. Zundel, *J. Chem. Soc., Faraday Trans*., 1995, **91**, 3831.
5 M. C. Etter, *J. Phys. Chem*., 1991, **95**, 4601.
6 J. Cirujeda, M. Mas, E. Molins, F. L. de Panthou, J. Laugier, J. G. Park, C. Paulsen, P. Rey, C. Rovira and J. Veciana, *J. Chem. Soc., Chem. Commun*., 1995, 709.
7 A. Izuoka, M. Fukada, R. Kumai, M. Itakura, S. Hikami and T. Sugawara, *J. Am. Chem. Soc*., 1994, **116**, 2609.
8 T. Okuno, T. Otsuka and K. Awaga, *J. Chem. Soc., Chem. Commun*., 1995, 827.
9 E. F. Ullman, J. H. Osiecki, D. G. B. Boocock and R. Darcy, *J. Am. Chem. Soc*., 1972, **94**, 7047.
10 G. M. Sheldrick, *Crystallographic Computing*, ed. G. M. Sheldrick, C. Kruger and R. Goddard, Oxford University Press, Oxford, 1985, p. 175.
11 P. T. Beurskens, G. Admiraal, G. Beurskens, W. P. Bosman, S. Garcia-Granda, R. O. Gould, J. M. M. Smits and C. Smykalla, *The DIRDIF program system, Technical Report of the Crystallography Laboratory*, University of Nijmegen, The Netherlands, 1992.
12 T. Sakurai and K. Kobayashi, *Rept. Inst. Phys. Chem. Res*., 1979, **55**, 69.
13 K. Awaga and Y. Maruyama, *Chem. Mater*., 1990, **2**, 535.
14 J. J. P. Stewart, *J. Comput. Chem*., 1989, **10**, 209.
15 T. Akita, Y. Mazaki and K. Kobayashi, *J. Chem. Soc., Chem. Commun*., 1995, 1861.
16 K. Awaga, T. Inabe and Y. Maruyama, *Chem. Phys. Lett*., 1992, **190**, 349.
17 H. M. McConnell, *J. Chem. Phys*., 1963, **39**, 1910.
18 S. L. Johnson and K. A. Rumon, *J. Phys. Chem*., 1965, **69**, 74.
19 K. Awaga, A. Yamaguchi, T. Okuno, T. Inabe, T. Nakamura, M. Matsumoto and Y. Maruyama, *J. Mater. Chem*., 1994, **4**, 1377.
20 K. Morokuna, *Acc. Chem. Res*., 1977, **10**, 294; N. Mataga and T. Kubota, *Molecular Interactions and Electronic Spectra*, Marcel Dekker, Inc., New York, 1970.
21 J. C. Bonner and M. E. Fisher, *Phys. Rev. A*, 1964, **135**, 640.
22 J. W. Hall, W. E. Marsh, R. R. Weller and W. E. Hatfield, *Inorg. Chem*., 1981, **20**, 1033.
23 K. Awaga, T. Okuno, A. Yamaguchi, M. Hasegawa, T. Inabe, Y. Maruyama and N. Wada, *Phys. Rev. B*, 1994, **49**, 3975.

Paper 7/08121I; *Received* 11*th November*, 1997